

Biofabrication of a Functional Tubular Construct from Tissue Spheroids Using Magnetoacoustic Levitational Directed Assembly

Vladislav A. Parfenov,* Elizaveta V. Koudan, Alisa A. Krokhmal, Elena A. Annenkova, Stanislav V. Petrov, Frederico D. A. S. Pereira, Pavel A. Karalkin, Elizaveta K. Nezhurina, Anna A. Gryadunova, Elena A. Bulanova, Oleg A. Sapozhnikov, Sergey A. Tsysar, Kaizheng Liu, Egbert Oosterwijk, Henk van Beuningen, Peter van der Kraan, Sanne Granneman, Hans Engelkamp, Peter Christianen, Vladimir Kasyanov, Yusef D. Khesuani, and Vladimir A. Mironov*

In traditional tissue engineering, synthetic or natural scaffolds are usually used as removable temporal support, which involves some biotechnology limitations. The concept of “scaffold” approach utilizing the physical fields instead of biomaterial scaffold has been proposed recently. In particular, a combination of intense magnetic and acoustic fields can enable rapid levitational bioassembly of complex-shaped 3D tissue constructs from tissue spheroids at low concentration of paramagnetic agent (gadolinium salt) in the medium. In the current study, the tissue spheroids from human bladder smooth muscle cells (mysospheres) are used as building blocks for assembling the tubular 3D constructs. Levitational assembly is accomplished at low concentrations of gadolinium salts in the high magnetic field at 9.5 T. The biofabricated smooth muscle constructs demonstrate contraction after the addition of vasoconstrictive agent endothelin-1. Thus, hybrid magnetoacoustic levitational bioassembly is considered as a new technology platform in the emerging field of formative biofabrication. This novel technology of scaffold-free, nozzle-free, and label-free bioassembly opens a unique opportunity for rapid biofabrication of 3D tissue and organ constructs with complex geometry.

1. Introduction

Despite recent serious advances in the field of tissue engineering, the creation of the multilayer complex tubular constructs is still a challenge.^[1] Many organ systems of the human body consist of tubular structures, especially cardiovascular, respiratory, urinary, and gastrointestinal systems. Historically, the development of tissue-engineered blood vessels (TEBV) predominates over other tubular tissue types. In 1986 Weinberg and Bell pioneered the TEBV by casting collagen with smooth muscle cells (SMCs) and fibroblasts in the tubular mold with subsequent culturing.^[2] Another approach—cell sheet assembly—was introduced in 1998 by L'Heureux et al., who wrapped cell sheets cultured of SMCs and fibroblasts around a mandrel to produce a multilayer TEBV.^[3] This approach was further modified and applied by several groups.^[4–6] In addition to TEBV, cell sheet technology

Dr. V. A. Parfenov, Dr. E. V. Koudan, Dr. E. A. Annenkova, S. V. Petrov, F. D. A. S. Pereira, A. A. Gryadunova, Dr. E. A. Bulanova, Y. D. Khesuani, Dr. V. A. Mironov
Laboratory for Biotechnological Research “3D Bioprinting Solutions”
Moscow 115409, Russia
E-mail: vapar@mail.ru; vladimir.mironov54@gmail.com
Dr. V. A. Parfenov
A. A. Baikov Institute of Metallurgy and Material Science
Russian Academy of Sciences
Moscow 119334, Russia

A. A. Krokhmal, Prof. O. A. Sapozhnikov, Dr. S. A. Tsysar
Department of Physics
Lomonosov Moscow State University
Moscow 119991, Russia

Dr. P. A. Karalkin, E. K. Nezhurina
P. A. Hertsen Moscow Oncology Research Center
National Medical Research Radiological Center
Moscow 125284, Russia

Dr. P. A. Karalkin, Dr. V. A. Mironov
I. M. Sechenov First Moscow State Medical University of the Ministry of Health of the Russian Federation (Sechenov University)
Moscow 119991, Russia

K. Liu, Prof. E. Oosterwijk
Department of Urology
Radboud University Medical Center
Nijmegen 9102, The Netherlands

 The ORCID identification number(s) for the author(s) of this article can be found under <https://doi.org/10.1002/adhm.202000721>

DOI: 10.1002/adhm.202000721

was also applied to create tubular genitourinary graft,^[7,8] urethra,^[9] and colon graft.^[6] Besides hydrogel casting and cell sheet technologies, the strategy based on the use of cell-laden scaffold material has been applied.^[10] In vascular tissue engineering, this approach has been explored for a wide range of materials, including synthetic polymers,^[10,11] natural polymers,^[12] decellularized porcine,^[13] or human organs.^[14] The use of cell-laden scaffold with tubular shape for urethral reconstruction has been reported in some preclinical^[15–17] and clinical studies.^[18]

3D bioprinting is an emerging technology that has the potential to create complex multilayer tissue constructs, as it provides control over the architecture of the construct by the automatic deposition process. Zhang et al. used 3D bioprinting technology to create a cell-laden urethra using synthetic biodegradable polymer, urothelial cells, and SMCs.^[19] Pi et al. applied microfluidic bioprinting to produce multilayer tubular urothelial and vascular tissue constructs.^[20] Meanwhile, Itoh et al. demonstrated an original method for the robotic-assisted assembly of tubular organs, in particular, vascular tissue utilizing the circle-shaped metal needles as a temporary framework for spheroids prepared from fibroblasts or SMCs. In this technology (called “Kenzan method”), patterned spheroids were then placed into a bioreactor to support their fusion process and finally to remove the needles from a mature rigid tubular construct.^[21,22] In another approach, proposed by Norotte et al., various vascular cell types were aggregated into discrete units, either multicellular spheroids or cylinders of controllable diameter, which then were printed layer-by-layer concomitantly with agarose rods, used here as a molding template. A unique aspect of this method was the ability to construct the hierarchical vessel trees, consisted of tubes with distinct diameters and shapes.^[23]

As an alternative to the scaffold-based approach, new scaffold-free technologies based on using physical fields as temporal support have been developed for the rapid fabrication of tissue constructs with complex geometry. Several research groups successfully applied acoustic waves as a tool for patterning cells and tissue spheroids into densely packed functional 3D tissue constructs, such as 3D cardiac tissue constructs,^[24] 3D ring-shaped tissue construct formed by fusion fibroblast and endothelial cells spheroids^[25] and 3D ring-shaped soft cellu-robots from neurons and astrocytes.^[26] Apart from the acoustic field, the principle of magnetic levitation can be also utilized as a patterning tool to produce complex 3D tissue structures. Magnetic levitational assembly, in turn, can be achieved either by using paramagnetic agents^[27–30] or magnetic nanoparticles entrapped by cells.^[31–33]

It should be noted that, unlike nanoparticles, paramagnetic agents could be easily removed from constructs at the end of the biofabrication process. However, high concentrations of gadolinium salts commonly applied as a paramagnetic agent for magnetic levitational assembly can also be toxic for cells.^[34,35]

In this study, we biofabricated viable tubular tissue constructs from human bladder SMCs tissue spheroids by combining magnetic levitational and acoustic assembly. Previously, we reported the assembly of ring-shaped tissue construct in the magnetoacoustic field^[36] generated with permanent magnets, using a very high, potentially toxic, concentration of gadolinium salts. Here, to achieve the magnetic levitational assembly at a low concentration of the paramagnetic medium, we once again used a 50 mm bore, 31 T Bitter magnets in High Field Magnet Laboratory, Radboud University, Nijmegen, the Netherlands as in our previous study.^[37]

Evaluation of the functional activity for tissue-engineered constructs containing contractile smooth muscle elements is an important stage of their testing at the preclinical stage. To do this, various biological and pharmacological constrictor agents, such as phenylephrine, prostaglandin, and adenine nucleotides, can be used.^[38,39] Recently, a high-throughput in vitro ring assay for vasoactivity using magnetic 3D bioprinting has been shown. The principle behind this assay is the magnetic printing of vascular SMCs into 3D rings, whose contraction can be altered by vasodilators and vasoconstrictors.^[40] In our study, we used endothelin-1 to demonstrate the viability and the contractility of tubular construct assembled in a high magnetic field using hybrid magnetoacoustic technology.

2. Results

2.1. Simulation of the Assembly Process

The conceptual flow chart of the experiment for levitational magnetic-acoustic fabrication of a construct from tissue spheroids is shown in **Figure 1**. The parameters for the magnetoacoustic levitational assembly of the ring- and tube-shaped tissue constructs were selected using computer modeling. The distribution of acoustic pressure generated by cylindrical piezoceramic transducer in the region of interest and its action on the particles is shown in **Figure 2a,b**. To predict the trajectories of particles moving in the magnetoacoustic field and to pattern the formation of a solid tube, the transient particle motion under all acting forces was simulated. As expected, particles collected in the nodes of standing acoustic waves levitated under the action of a magnetophoretic force and formed a solid tube with a radius equal to the first standing field node radius. The results of numerical simulation (**Figure 2c–e**) were reproduced in the experiment. The shape of the fabricated tissue construct was in good agreement with the results of the simulation.

2.2. The Effect of Gadobutrol on Viability and Biomechanical Properties of Tissue Spheroids

For magnetoacoustic levitational assembly of 3D tubular tissue-engineered constructs, we used contractile biologic objects

H. van Beuningen, P. van der Kraan
Department of Experimental Rheumatology
Radboud University Medical Center
Nijmegen 9102, The Netherlands

Dr. S. Granneman, Dr. H. Engelkamp, Prof. P. Christianen
High Field Magnet Laboratory (HFML-EMFL)
Radboud University
Toernooiveld 7, Nijmegen 9010, The Netherlands

Prof. V. Kasyanov
Riga Stradins University
Riga, LV-1007, Latvia

Prof. V. Kasyanov
Riga Technical University
Riga, LV-1658, Latvia

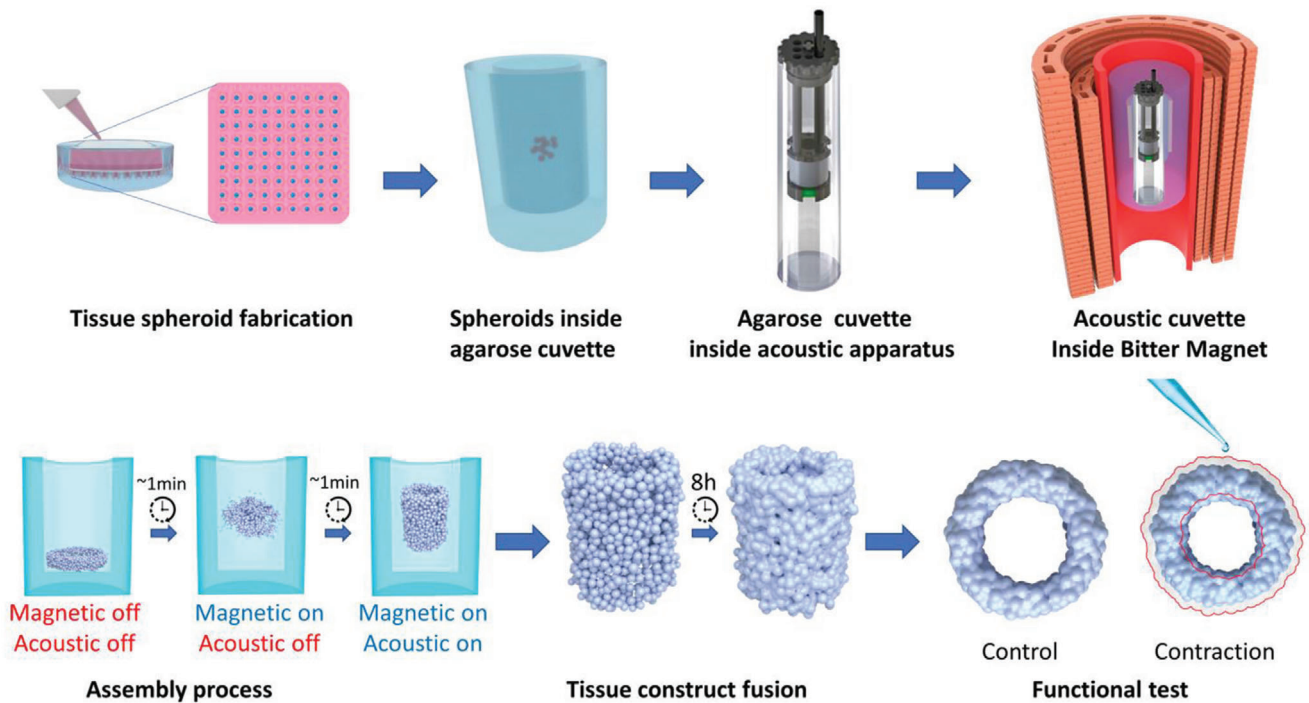


Figure 1. The conceptual flow chart of the experiment for levitational magnetic-acoustic fabrication of a construct from tissue spheroids.

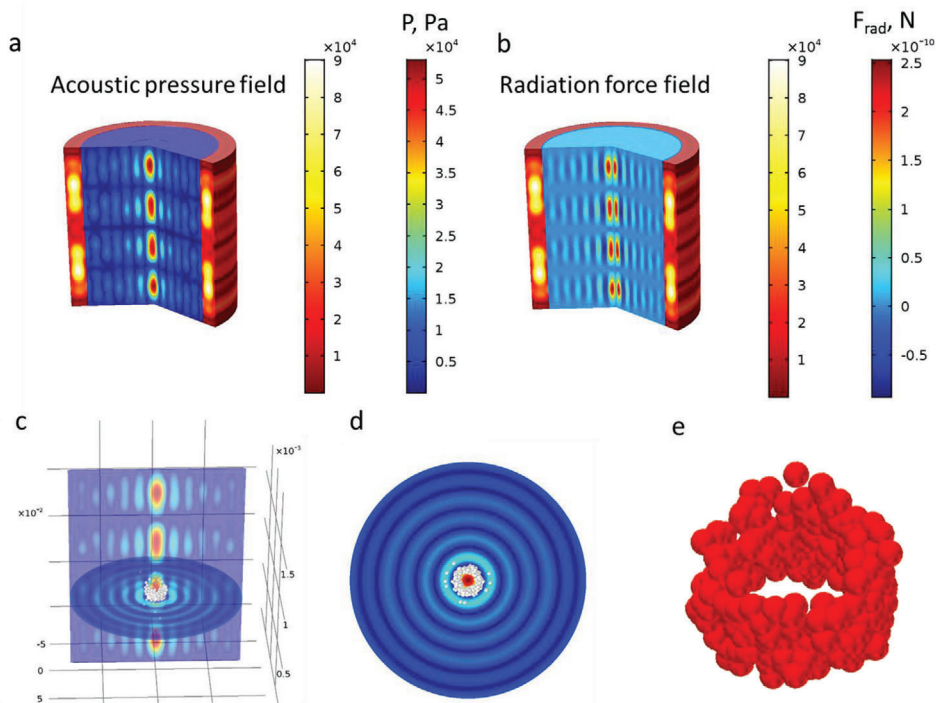


Figure 2. Results of numerical modeling of the acoustic standing field and the process of the construct assembly in the magnetoacoustic field: a) distribution of acoustic pressure amplitude inside the transducer, b) distribution of radiation force magnitude, c) illustration of particles accumulation in the nodes of acoustic pressure field, d) a coaxial structure of standing wave nodes inside the cylindrical transducer, and e) the resulting tubular assembly, obtained in the magnetoacoustic field as a result of particle motion tracing.

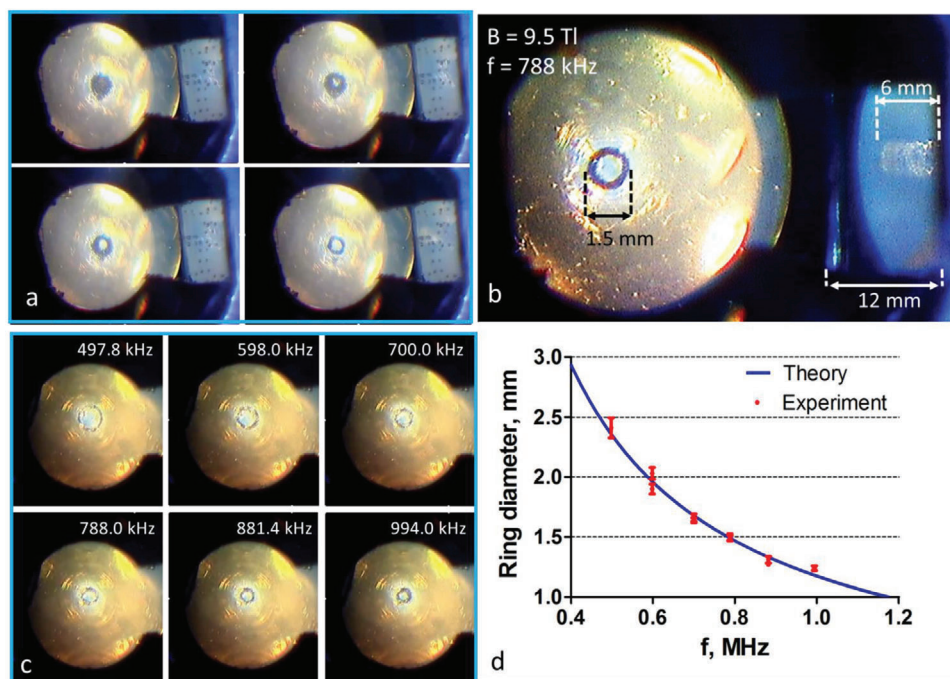


Figure 3. The biofabrication of the construct from tissue spheroids at different parameters of the acoustic field: a) the process of ring assembly in a levitational state utilizing acoustic and magnetic fields, b) the levitating tubular construct, c) the change in the diameter of the construct depends on the frequency, and d) the convergence of the experimental and simulation diameter on frequency dependence ($n = 7$).

whose functionality could be further validated. Thus, we selected human bladder SMCs (hbSMCs) that contract in response to endothelin-1 and other agents.^[41] Tissue spheroids with regular size and shape were prepared using MicroTissues 3D Petri dish micromolds (Figure S1a,b, Supporting Information). The average 1 d old spheroid diameter was $454 \pm 25 \mu\text{m}$. The average spheroid roundness was 0.93 ± 0.04 .

First, we estimated the influence of gadobutrol on the viability and mechanical properties of tissue spheroids (Figure S1c,d, Supporting Information). The viability of cells within tissue spheroids was analyzed using the CellTiter-Glo 3D kit based on bioluminescent Adenosine triphosphate (ATP) detection in viable cells. At $20 \times 10^{-3} \text{ M}$ gadobutrol tissue spheroids demonstrated almost 100% viability, whereas $50 \times 10^{-3} \text{ M}$ gadobutrol caused the viability decrease to 87% (Figure S1c, Supporting Information). The significant toxic effect on tissue spheroids was revealed at $250 \times 10^{-3} \text{ M}$ gadobutrol. It is worth mentioning that the mechanical properties of tissue spheroids directly depend on their viability. In particular, the increase in the internal content of dead cells reduces the elastic properties (elastic modulus or Young's modulus), which can be measured using standard methods of tensiometry. Earlier, we revealed a similar correlation for spheroids prepared from sheep chondrocytes (chondrospheres).^[30] The influence of gadobutrol on mechanical properties of tissue spheroids prepared from hbSMCs in the current study was also estimated by tensiometry using microsquisher with parallel plates modification. As shown in Figure S1d in the Supporting Information, 20×10^{-3} and $50 \times 10^{-3} \text{ M}$ gadobutrol did not alter tissue spheroids biomechanics, while the increase of gadobutrol concentration up to $250 \times 10^{-3} \text{ M}$ re-

sulted in a significant decrease of elastic modulus value, evidently caused by the toxic effect of gadobutrol.

We also investigated the dynamics of spheroids fusion in the presence of different gadobutrol concentrations for 24 h (Figure S2, Supporting Information) as tissue level biomarker of tissue spheroids viability. The intersphere angle, contact length, and doublet length were measured according to the method described by Susienka et al.^[42] All spheroids pairs demonstrated approximately the same rates of fusion regardless of the presence of gadobutrol. Contact length gradually increased as a function of time and after 24 h it was equal to the initial diameter of a single spheroid. At the same time, the growth of contact length for spheroid doublets in $50 \times 10^{-3} \text{ M}$ gadobutrol was slightly slower than one for spheroid doublets in $20 \times 10^{-3} \text{ M}$ gadobutrol and without the addition of gadobutrol. Intersphere angle increased up to 160° , indicating almost complete spheroid fusion. Double length shortened gradually and represented 72% of the original value after 24 h of incubation.

2.3. Assembly of 3D Tissue Constructs in a High Magnetic and Acoustic Fields

We achieved the levitation of the tissue spheroids in a high magnetic field with an intensity of 9.5 T. After the generation of the acoustic field, levitating tissue spheroids started to assemble into ring-shaped and tubular structures (Figure S3, Supporting Information). Figure 3a demonstrates the transformation of the randomly distributed particles to the ring by gradually adjusting the amplitude of the acoustic wave, thus, changing the intensity of

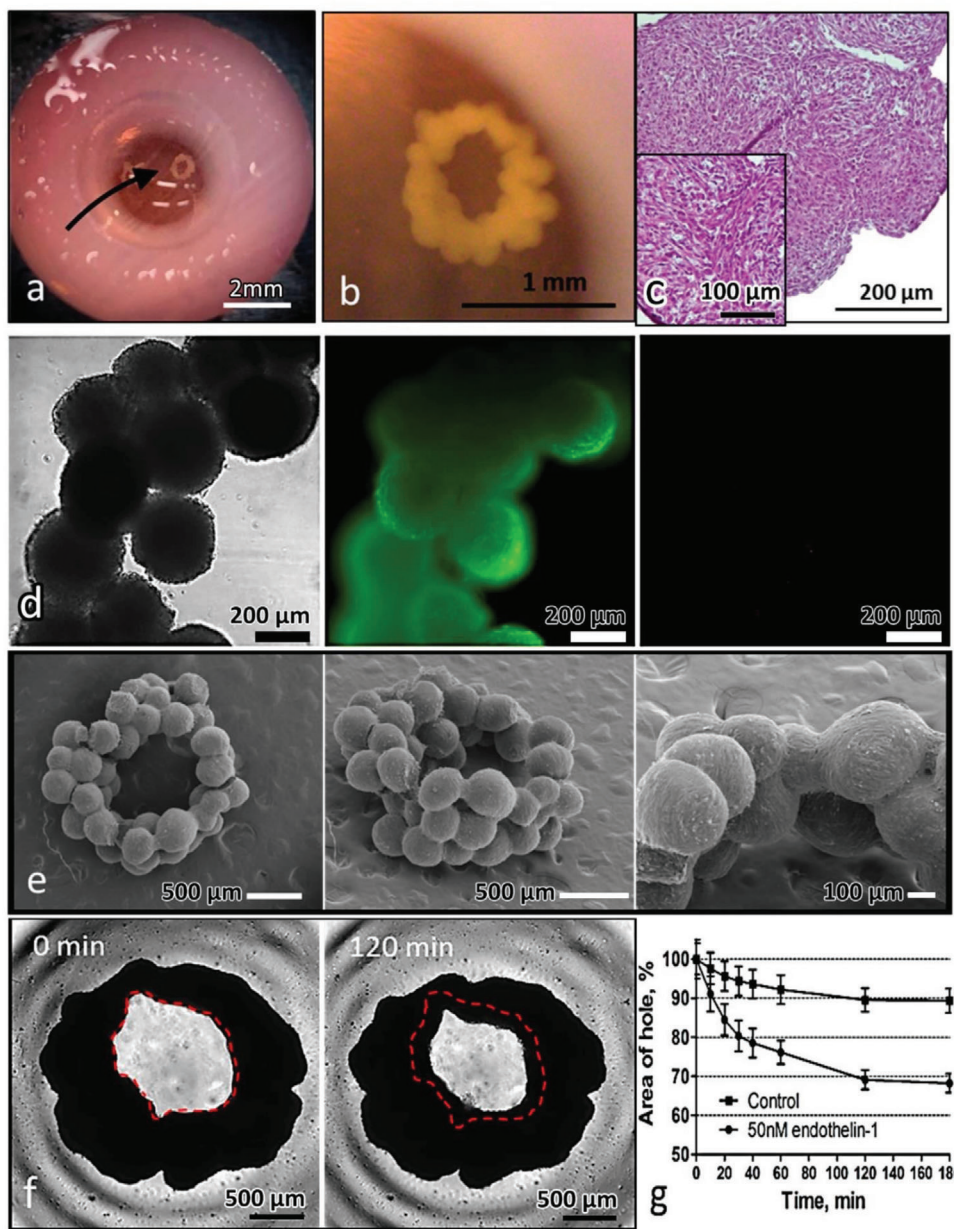


Figure 4. The characterization of tubular construct biofabricated by magnetoacoustic levitation during 8 h at 20×10^{-3} M gadobutrol: a) photograph of construct inside of agarose cuvette, b) a stereo image of the construct, c) histology of construct, d) Live/Dead assay of construct: phase contrast, calcein-AM (green) and propidium iodide (red) from left to right, e) SEM of the construct, f) a contraction of the construct during 120 min in the presence of 50×10^{-9} M endothelin-1, and g) the dynamic of area decrease caused by 50×10^{-9} M endothelin-1 ($n = 3$).

the acoustic radiation force. The height of the construct depended on the number of particles initially placed in the cuvette. Figure 3b shows the resulting tubular construct (bottom view and side view through the system of mirrors), observed at several frequencies. Stepwise change of resonance frequency led to the shift in ring-shape construct diameter (Figure 3c and Video S1, Supporting Information). Thus, we were able to regulate the parameters of the assembly to obtain the desired size of the construct. The dependence of the assembly diameter on the frequency was measured in the experiment (Figure 3d) and corresponded well to the theoretical evaluation (see the Supporting Information).

Figure 4a,b shows tubular tissue construct created from tissue spheroids after 8 h of magnetoacoustic levitational assembly. It should be noted that during the levitation for 8 h, the tubular tissue constructs underwent subtle changes in size (some thinning of the wall thickness) due to the process of tissue spheroids fusion, but this did not affect their stable retention by the acoustic field. To evaluate cell viability in the biofabricated tissue construct, we performed histology analysis and Live/Dead assay (Figure 4c,d). The construct consisted of viable cells tightly packed inside tissue spheroids. Scanning electron microscopy (SEM) analysis proved the fusion of tissue spheroids into the

tubular 3D tissue constructs. As shown in Figure 4e, the constructs consisted of three layers of spheroids. The surface of spheroids exhibited the typical morphology of myospheres. It should be noted that the incubation time in the magnetoacoustic field was insufficient for the full spheroids fusion; therefore, the contours of individual spheroids were distinguishable. However, the constructs had a whole structure with enough physical strength for subsequent manipulations.

2.4. Functional Testing of 3D Tissue Constructs

To evaluate the ability of hbSMCs within biofabricated tissue to constrict in response to the addition of physiological vasoconstrictor, we incubated them with 50×10^{-9} M endothelin-1. As shown in Figure 4f,g, the agent induced a time-dependent decrease in the area of construct inner hole, indicating that the contractile response had occurred. The lumen area reduction is an indicative parameter for the *in vitro* model of a hollow organ with a muscle wall. In our experiments, the lumen significantly decreased after the constrictor addition—up to 70% from the initial diameter, compared to the intact control—90%. Most of the reduction in the area occurred within the first 120 min after endothelin-1 addition. Incubating for another 60 min did not lead to further contraction. Thus, we demonstrated the functional activity of tubular hollow tissue-engineered construct.

3. Discussion

The main idea of the current work was the development and experimental validation of novel biofabrication technology—magnetoacoustic levitational bioassembly of 3D tissue-engineered constructs. Although there is a growing list of published papers about discrete magnetic or acoustic levitational bioassembly, it is the first report to the best of our knowledge about hybrid magnetoacoustic levitational bioassembly of functional human tissues. To develop the named approach, in this study we carried out the following technological steps: i) developing the hardware that enabled magnetoacoustic levitational bioassembly, ii) performing mathematical modeling and realized formative biofabrication of complex biological structures such as rings or tubes, and iii) testing the functionality of biofabricated 3D tissue-engineered tubular construct.

Previously we have already described the magnetic levitational bioassembly of spherical nonhollow 3D tissue construct from spheroids consisted of a human chondrosarcoma cells.^[37] Obtained data confirmed the preservation of cell spheroids viability and their fusion ability in a high magnetic field in the presence of Gd^{3+} salts. In the current study, we designed a custom agarose cuvette enabling biofabrication of tubular construct and theoretically more complex geometric forms using the acoustic field. Moreover, the assembly of a tissue construct in a magnetoacoustic field hardly could be possible without preliminary mathematical modeling, which allowed us to predict the rate of assembly and to optimize the range of experimental conditions in a situation with rather high consumption of resources, mainly electricity, by unique magnet infrastructure of European magnetic field laboratory.

The widespread occurrence of congenital or acquired defects in the urinary system resulting from injuries or degenerative diseases determines the stable need for the creation of tissue-engineered implants (such as urethral grafts) suitable for reconstructive plastic surgery.^[9,19,20] Nowadays, it has become apparent that the use of cellular components is crucial for restoring the architectonics and functional activity of substituted tissues. Thus, it was shown that cell-seeded (with autologous bladder epithelial and SMCs) tubular collagen scaffolds can be used to repair long urethral defects, whereas scaffolds without cells lead to poor tissue development and strictures.^[17] In the current study, we fabricated a tubular 3D tissue construct from human bladder SMCs. The resulted construct consisted of three layers of spheroids, which theoretically can form three muscle layers of the wall of a mature bladder—external longitudinal, middle circular, and internal oblique—if appropriate conditions for its postassembly maturation would be created. In follow-up studies, we plan to add spheroids from urogenital epithelial cells to mimic the structure of the natural urinary system walls. Although we have focused on the creation of tissue construct from hbSMCs, we suppose that our approach could also be applied to other tubular structures such as blood vessels, colon, and trachea.

In terms of biofabrication, besides the assessing of viability and morphological characteristics, the most important property for the tubular constructs assembled from SMCs spheroids is the confirmation of their functional activity. Thus, the capacity of muscular tubular constructs to contract in the presence of vascular constrictors or relax in the presence of vasodilator is considered as a proof of its functionality.^[42,43] In our study, the tubular construct fabricated from hbSMCs also responded to the stimuli of vasoconstrictor endothelin-1. Such effects of assembled smooth muscle tissue can be utilized as a potentially very predictive *in vitro* model for testing new cures for bronchial asthma, vascular hypertension, and erectile dysfunction. This approach can be especially useful, given that animal models are sometimes not suitable for testing novel drugs because they do not have corresponding surface cellular receptors repertoire typical for human SMCs.^[44]

One of the main problems in the design of tubular organs is still the difficulty of obtaining complex geometry that mimics the structure of native tissues. It is especially true for the formation of the microscale cell layers organization and the extracellular matrix production, which are necessary to recreate the complex anatomical architecture of the tubular organ networks having multiple bifurcations or physiological thickenings in the regions of maximum hydrostatical pressure.^[45]

The proposed method of hybrid magnetoacoustic levitation bioassembly is aimed at overcoming existing technological barriers. In particular, the spatial distribution of biological objects could be determined only by the applied fields, and compared with traditional methods of biofabrication, it does not depend on the physicochemical properties of biomaterials included in scaffolds or “bio-ink” compound. Thus, the magnetoacoustic bioassembly method can be considered as a consistent extension of the “scaffold” concept, when only physical fields are used for temporary support of cells or their aggregates. Moreover, this approach makes it possible to abandon the use of natural or synthetic biomaterials completely, the clinical use of which is still associated with the risks of developing immunological

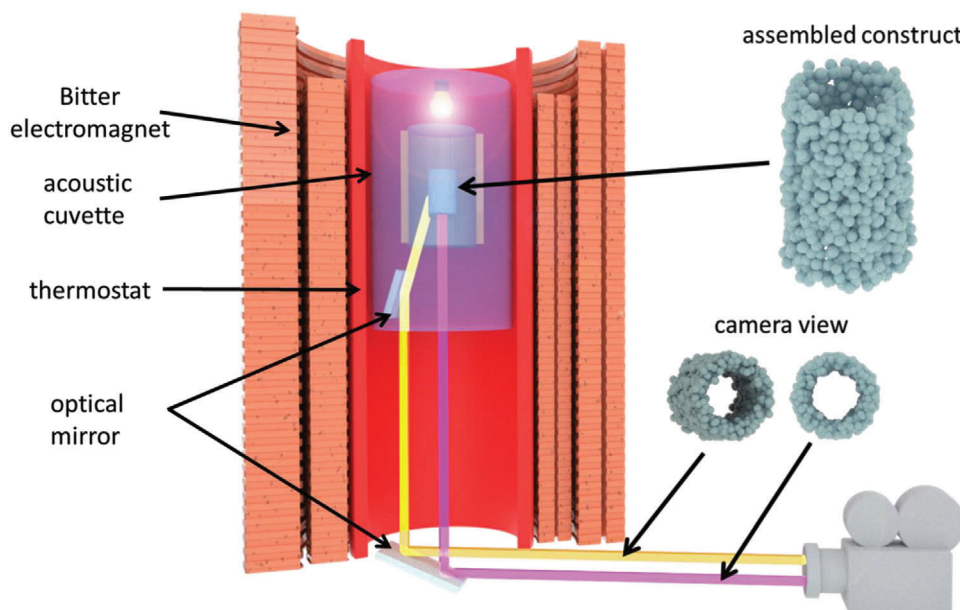


Figure 5. The optical scheme used for the registration of the construct assembly in the magnetoacoustic setting.

rejection or imperfect resorption, often causing the development of inflammatory reactions or fibrosis in the recipient's body.

Thus, further development of the magnetoacoustic levitation bioassembly seems to be reasonable and could be facilitated by both improving the technological settings of the magnetoacoustic devices as well as by complementing them with flow bioreactor systems to support the fusion of spheroids thus formatting the physiological and structural determinants in the resulting tissue constructs.

4. Conclusions

In the current study, we have realized the hybrid magnetoacoustic levitational bioassembly of 3D functional tubular tissue-engineered constructs from hbSMCs myospheres. In general, our experiments gave the proof-of-concept for utilizing the solid scaffold-free, nozzle-free, and label-free magnetoacoustic levitation bioassembly for rapid biofabrication of tissue and someday organ constructs with complex geometry. Further scaling of the technology and development of conveying flow bioreactor systems will approach the creation of personalized implants corresponding to the anatomical and physiological characteristics of the patient's organs in order to improve the clinical outcome. Overall, the hybrid magnetoacoustic levitational bioassembly comprises a new emerging technology platform in the rapidly evolving field of formative biofabrication.

5. Experimental Section

Magnetoacoustic Setup: To enable magnetic levitation, a 50 mm bore 31 Tesla Bitter magnet was used (Figure 5).^[46] The monitoring technique of the assembly process by using a system of mirrors and a digital camera

is shown in Figure 5. For the biofabrication process, a cuvette contained piezoceramic cylindrical and ring-shaped ultrasonic transducers, light-emitting diodes, an optical mirror for monitoring, and agarose container for tissue spheroids was designed (Figure 6a–c). The detailed description of the experimental setup construction is available in the Supporting Information. Piezoceramic cylindrical transducer generated standing ultrasound waves at frequencies, providing the assembly of tissue spheroids into the ring- and tube-shaped tissue constructs. The ring-shaped transducer coupled with focusing parabolic plate, placed above the cylinder transducer, and focused inside its hollow space was used to provide mixing of tissue spheroids before the initiation of the assembly process (Figure S3, Supporting Information).

The agarose container with tissue spheroids and culture medium containing 20×10^{-3} M gadobutrol (Figure 6d) was placed inside the cylindrical transducer, as shown in Figure 6e. The agarose density and sound speed are very close to water values, so the use of the agarose container instead of traditional plastic or glass was essential to avoid additional wave reflection and distortion. The assembled cuvette was placed inside the Bitter magnet (Figure 6f,g) with the magnetic field intensity ≈ 9.5 T. The formation of the ring- and tube-shaped structures of different diameters was achieved by the application of acoustic waves with several resonant frequencies in the range from 0.5 to 1 MHz. The nominal amplitude of the acoustic wave at the outlet of the generator was up to 10 V.

To create the most efficient standing wave by the cylindrical transducer, the resonance of the system was reached and a maximum of output power at the same time was achieved. Putting the transducer inside the cuvette and adding the culture flask and reflector into the system could change the electric power function of the frequency and shift resonances. The frequency dependence of the transducer electric power was measured to adjust parameters of the maximum power. It was found that the maximum of the transducer emitted energy corresponded to the frequency 0.64 MHz, and also, the number of secondary resonances exists (Figure 6h). This frequency set communicated to various configurations of standing ultrasound field and allowed the creation of tubular constructs with different diameters (see the Supporting Information).

After the assembly, tissue construct was held in the maintaining magnetoacoustic field for 8 h to complete the fusion of tissue spheroids. At the end of the biofabrication process, the obtained tissue construct was carefully transferred from the magnetoacoustic setup to culture plates for further functionality testing and histological analysis.

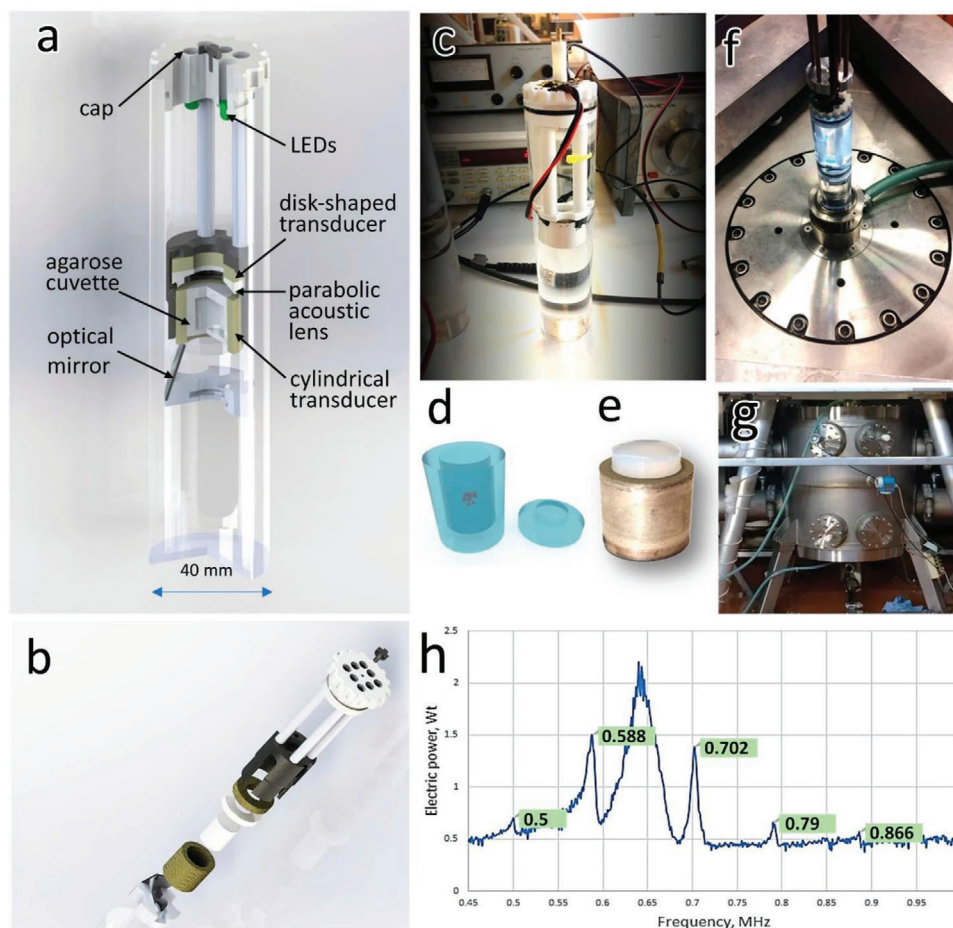


Figure 6. The construction of cuvette with acoustic transducers: a) the scheme of the cuvette (offset section), b) the scheme of the cuvette with separated elements, c) the cuvette fulfilled with liquid, d) 3D model of agarose cuvette with tissue spheroids inside, e) agarose cuvette inside the cylindrical transducer, f) the installation of the cuvette in the Bitter magnet, g) the Bitter magnet, used in experiments (side view), and h) the frequency dependence of the transducer electric power at an ideal load of 50 Ω . Profile peaks correspond to the resonance frequencies. Assembly of particles was performed near these frequencies.

Numerical Simulation of Assembly: Calculation of the Magnetic Field, Acoustic Field, Dynamics of Particle Motion: The design of the experimental setup was based on the numerical simulation results. Such estimates were necessary to determine the ultrasound pressure distribution and to simulate the action of acoustic radiation and magnetophoretic forces. Estimation of the optimal parameters for the experiment was performed by the finite element method using the COMSOL Multiphysics and Matlab software. A radially polarized piezoelectric cylinder created the acoustic field with internal and external radii of respectively 8 and 10 mm and 20 mm in length. In the experiment, the spheroids localized in the inner region of the piezoelectric cylinder, so it was necessary to obtain a high level of homogeneity of the field in the vertical direction. However, the real field structure was not entirely homogeneous: surface acoustic waves inevitably arise at the transducer-liquid boundary, and this fact with even small defects of the transducer surface, in turn, leads to variations of the amplitude of the acoustic pressure.^[47] The installation length of 30 cm was chosen to reduce the reflection from its sides, which potentially could disrupt the structure of the standing wave inside the piezoelectric cylinder.

Based on the resulting acoustic pressure field, the Gor'kov radiation force, acting on a spherical particle placed in an acoustic field, was found.^[48,49] The properties of the model particles corresponded to the physical characteristics of real tissue spheroids (ultrasound velocity was 1600 m s⁻¹ as for muscle tissue,^[50] the density was 1050 kg m⁻³, and the diameter was 0.2 mm).

The distribution of the magnetic field was taken from the experimental data of the previous study,^[37] while the magnetic field was varying along the vertical axis. The magnetophoretic force was calculated according to previous settings^[37] with the current experimental parameters: relative magnetic permeability of spheroids and medium were $\mu_{\text{sph}} = 0.999992$ and $\mu_f = 0.999994$, respectively, the intensity of the magnetic field was 9.5 T.

The particle trajectories were calculated by solving the dynamic equations of motion under the action of the acoustic radiation force, the magnetophoretic force, the Stokes drag force, the elastic force of particle-particle interaction, and the gravity force.

Cell Culture: hbSMCs were purchased from ScienCell (Cat. No. 4310) and cultured in serum-free medium for SMCs with growth supplements (Cat. No. 1101, ScienCell, USA). The cells were incubated at 37 °C in a humidified atmosphere with 5% CO₂ and routinely splitted at 85–95% confluence. Single-cell suspension preparation was performed using mild enzymatic dissociation with a 0.25% trypsin/0.53 × 10⁻³ m Ethylenediaminetetraacetic acid (EDTA) solution (Cat. No. P043p, Paneco, Russia). Cells were free of mycoplasma contamination as verified using the 4',6-Diamidino-2-Phenylindole (DAPI). (Cat. No. D1306, Invitrogen, USA) staining protocol.

Formation of Tissue Spheroids Using MicroTissues 3D Petri Dishes: The tissue spheroids were routinely prepared using MicroTissues 3D Petri dish micromolds (Z764019-6EA, 81 circular wells 800 μm × 800 μm ,

Sigma-Aldrich, USA) according to manufacturing protocol. Briefly, hbSMC cells were harvested from the culture flasks and then suspended in cell culture medium at the concentration of 6.8×10^6 cells per milliliter. After that, 190 μL of suspension was placed into each 81-well nonadhesive agarose mold, and molds were placed in 12-well culture plates (Nunc, USA) and covered with complete growth media after 1 h. The resultant tissue spheroids contained 1.6×10^4 cells.

Spheroid Fusion Assay: Spheroid fusion assay was performed using ultralow-adhesive spheroid microplates (Cat. No. 4520 Corning, USA). Pairs of 1 d old tissue spheroids (16 000 cells per spheroid) were placed together in the wells and incubated with 0, 20×10^{-3} , and 50×10^{-3} m gadobutrol (Gd-DO3A-butrol, "Gadovist", Bayer Pharma AG, Germany) for 24 h. Bright-field images of spheroid doublets were obtained at points 0, 2, 4, 6, and 24 h using Nikon Eclipse Ti-S microscope (Figure S4, Supporting Information). Contact length, intersphere angle, and doublet length were measured using Image J 1.48v software (The National Institutes of Health (NIH), Bethesda, MD, USA) and plotted as a function of time using GraphPad Prism software (GraphPad Software, Inc., La Jolla, CA).

Determination of Spheroid Diameter and Roundness Distribution: Tissue spheroids were biofabricated and captured at 1st day using bright-field imaging at inverted microscope Nikon Eclipse Ti-S, Japan. Spheroid diameters and roundness were measured using Image J 1.48v software (NIH, Bethesda, MD, USA). Briefly, all original grayscale images were converted to simplified threshold images under the same converting condition and the edges of the spheroids were automatically detected. MinFerret's diameters of the exposed spheroid edges were measured initially as pixels and converted to micrometers by comparing it to a reference length. Roundness was measured using Image J 1.48v shape descriptor and calculated using Equation (1)

$$\frac{4 * \text{area}}{\pi * (\text{major axis})^2} \quad (1)$$

Estimation of Tissue Spheroids Viability at Different Concentrations of Gadobutrol: The viability of tissue spheroids was assessed using the CellTiter-Glo 3D kit (Cat. No. G9682, Promega, USA) according to the manufacturer protocol. 1 d old tissue spheroids (16 000 cells per spheroid) were exposed to 0, 20×10^{-3} , 50×10^{-3} , and 250×10^{-3} m gadobutrol for 24 h. Then CellTiter-Glo 3D kit was added and luminescence was recorded after 60 min incubation using VICTOR X3 Multilabel Plate Reader (Perkin Elmer, USA).

Live/Dead Assay: Cell viability within tubular construct made from hbSMC spheroids was monitored using the Live/Dead Cell Double Staining Kit (Cat. No. 04511, Sigma-Aldrich, USA) according to the manufacturer's protocol after 8 h of incubation in a high magnetic field. The tubular construct was incubated with a solution containing Calcein acetoxymethyl (AM) and propidium iodide (PI) at 37 °C for 30 min. After washing with Dulbecco's phosphate-buffered saline (PBS, Cat. No. 18912-014, Gibco, USA) the tubular construct was visualized by fluorescent microscopy (Nikon Eclipse Ti-S, Japan).

Histological Analysis: After assembly in a high magnetic field, samples were fixed in PBS-buffered 4% paraformaldehyde solution (Cat. No. P6148, Sigma-Aldrich), then put in melted 2% agarose gel (Cat. No. Am-0710-0.1, Helicon, Russia), and finally embedded in paraffin (Merck, Germany). Dewaxing was carried out using xylene and a battery of downstream alcohols. Serial sections with a thickness of 4 μm were cut with Microtome Microm HM355S (Thermo Fisher Scientific, USA), mounted on poly-L-lysine coated glass, and routinely stained with hematoxylin-eosin (Sigma-Aldrich, Germany).

SEM: Tubular construct made from hbSMC spheroids was fixed with PBS containing 2.5 v/v% glutaraldehyde (Cat. No. G5882, Sigma-Aldrich, USA), dehydrated through ethanol series, and then was dried in a critical point dryer (HCP-2, Hitachi Koki Co. Ltd., Japan). The sample was transferred on a stub of metal with an adhesive surface, coated with gold using ion coater (IB-3, EIKO, Japan), and then observed using the microscope JSM-6510 LV (JEOL, Japan).

Mechanical Testing: The mechanical properties of tissue spheroids were measured using a microscale parallel-plate compression testing system Microsquisher (CellScale, Canada) with associated SquisherJoy software. Tissue spheroids (16 000 cells per spheroid) were prepared using MicroTissues 3D Petri dish micromolds. 1 d old tissue spheroids were exposed to 0, 20×10^{-3} , 50×10^{-3} , and 250×10^{-3} m gadobutrol for 24 h before mechanical characterization. For mechanical testing, spheroids were placed in a PBS-filled bath at 37 °C and compressed to 50% deformation in 20 s. The microbeam with diameters 304.8 μm (recommended max force 917 mN) was employed. The force–displacement data obtained from the compression test were converted to stress–strain curves, and the lower portion of the curve (0–20% strain) was used to obtain a linear regression line and estimate Young's modulus. In each group, eight samples of spheroids were measured.

Tubular Construct Contraction Assay: The tubular construct was treated with 50×10^{-9} m endothelin-1 (Cat. No. E7764, Sigma-Aldrich, USA). The contraction of the construct was registered at points 0, 10, 20, 30, 40, 60, 120, and 180 min using the Nikon Eclipse Ti-S microscope. The area of tubular construct's inner hole was measured using Image J 1.48v software (NIH, Bethesda, MD, USA) and plotted as a function of time using GraphPad Prism software (GraphPad Software, Inc., La Jolla, CA).

Data Analysis: Statistical data were analyzed using GraphPad Prism software (GraphPad Software, Inc., La Jolla, CA) and represented as mean \pm the standard error of the mean (S.E.M). The analysis of variance test was used to find the significant differences between the means of the three and more groups with P -value < 0.0001 .

Supporting Information

Supporting Information is available from the Wiley Online Library or from the author.

Acknowledgements

V.A.P. and E.V.K. contributed equally to this work. This work was supported by HFML-RU/NWO-I, member of the European Magnetic Field Laboratory (EMFL), and Russian Foundation for Basic Research (RFBR), according to the Research Project No. 18-29-11076.

Conflict of Interest

The authors declare no conflict of interest.

Keywords

levitation assembly, magnetoacoustic biofabrication, myospheres, tissue spheroids, urethral grafts

Received: April 29, 2020

Revised: July 6, 2020

Published online:

- [1] J. Basu, J. W. Ludlow, *Trends Biotechnol.* **2010**, *28*, 526.
- [2] C. B. Weinberg, E. Bell, *Science* **1986**, *231*, 397.
- [3] N. L'heureux, S. Pâquet, R. Labbé, L. Germain, F. A. Auger, *FASEB J.* **1998**, *12*, 47.
- [4] D. Seliktar, R. A. Black, R. P. Vito, R. M. Nerem, *Ann. Biomed. Eng.* **2000**, *28*, 351.
- [5] H. Kubo, T. Shimizu, M. Yamato, T. Fujimoto, T. Okano, *Biomaterials* **2007**, *28*, 3508.
- [6] R. Othman, G. E. Morris, D. A. Shah, S. Hall, G. Hall, K. Wells, K. M. Shakesheff, J. E. Dixon, *Biofabrication* **2015**, *7*, 025003.

- [7] V. Cattani, G. Bernard, A. Rousseau, S. Bouhout, S. Chabaud, F. A. Auger, S. Bolduc, *Eur. Urol.* **2011**, *60*, 1291.
- [8] M. J. J. van Velthoven, R. Ramadan, F. S. Zügel, B. J. Klotz, D. Gawlitza, P. F. Costa, J. Malda, M. Castilho, L. M. O. de Kort, P. de Graaf, *Tissue Eng., Part C* **2020**, *26*, 190.
- [9] S. Zhou, R. Yang, Q. Zou, K. Zhang, T. Yin, W. Zhao, J. G. Shapter, G. Gao, Q. Fu, *Theranostics* **2017**, *7*, 2509.
- [10] R. L. E. Niklason, J. Gao, W. M. Abbott, K. K. Hirschi, S. Houser, R. Marini, L. E. Niklason, J. Gao, W. M. Abbott, K. K. Hirschi, S. Houser, R. Marini, R. Langer, *Science* **1999**, *284*, 489.
- [11] N. Hibino, E. McGillicuddy, G. Matsumura, Y. Ichihara, Y. Naito, C. Breuer, T. Shinoka, *J. Thorac. Cardiovasc. Surg.* **2010**, *139*, 431.
- [12] S. C. Schutte, Z. Chen, K. G. M. Brockbank, R. M. Nerem, *Tissue Eng., Part A* **2010**, *16*, 3149.
- [13] B. W. Tillman, S. K. Yazdani, L. P. Neff, M. A. Corriere, G. J. Christ, S. Soker, A. Atala, R. L. Geary, J. J. Yoo, *J. Vasc. Surg.* **2012**, *56*, 783.
- [14] M. Olausson, P. B. Patil, V. K. Kuna, P. Chougule, N. Hernandez, K. Methe, C. Kullberg-Lindh, H. Borg, H. Ejnell, S. Sumitran-Holgersson, *Lancet* **2012**, *380*, 230.
- [15] L. R. Versteegden, K. A. van Kampen, H. P. Janke, D. M. Tiemessen, H. R. Hoogenkamp, T. G. Hafmans, E. A. Roozen, R. M. Lomme, H. van Goor, E. Oosterwijk, W. F. Feitz, T. H. van Kuppevelt, W. F. Daamen, *Acta Biomater.* **2017**, *52*, 1.
- [16] R. E. De Filippo, B. S. Kornitzer, J. J. Yoo, A. Atala, *J. Tissue Eng. Regen. Med.* **2015**, *9*, 257.
- [17] H. Orabi, T. AbouShwareb, Y. Zhang, J. J. Yoo, A. Atala, *Eur. Urol.* **2013**, *63*, 531.
- [18] A. Raya-Rivera, D. R. Esquiliano, J. J. Yoo, E. Lopez-Bayghen, S. Soker, A. Atala, *Lancet* **2011**, *377*, 1175.
- [19] K. Zhang, Q. Fu, J. Yoo, X. Chen, P. Chandra, X. Mo, L. Song, A. Atala, W. Zhao, *Acta Biomater.* **2017**, *50*, 154.
- [20] Q. Pi, S. Maharjan, X. Yan, X. Liu, B. Singh, A. M. van Genderen, F. Robledo-Padilla, R. Parra-Saldivar, N. Hu, W. Jia, C. Xu, J. Kang, S. Hassan, H. Cheng, X. Hou, A. Khademhosseini, Y. S. Zhang, *Adv. Mater.* **2018**, *30*, 1706913.
- [21] M. Itoh, K. Nakayama, R. Noguchi, K. Kamohara, K. Furukawa, K. Uchihashi, S. Toda, J. I. Oyama, K. Node, S. Morita, *PLoS One* **2015**, *10*, e0136681.
- [22] N. I. Moldovan, N. Hibino, K. Nakayama, *Tissue Eng., Part B* **2017**, *23*, 237.
- [23] C. Norotte, F. S. Marga, L. E. Niklason, G. Forgacs, *Biomaterials* **2009**, *30*, 5910.
- [24] V. Serpooshan, P. Chen, H. Wu, S. Lee, A. Sharma, D. A. Hu, S. Venkatraman, A. V. Ganesan, O. B. Usta, M. Yarmush, F. Yang, J. C. Wu, U. Demi, S. M. Wu, *Biomaterials* **2017**, *131*, 47.
- [25] Y. Zhu, V. Serpooshan, S. Wu, U. Demirci, P. Chen, S. Güven, *Methods Mol. Biol.* **2019**, *1576*, 301.
- [26] T. Ren, P. Chen, L. Gu, M. G. Ogut, U. Demirci, *Adv. Mater.* **2020**, *32*, 1905713.
- [27] E. Türker, N. Demirçak, A. Arslan-Yildiz, *Biomater. Sci.* **2018**, *6*, 1745.
- [28] M. Anil-Inevi, S. Yaman, A. A. Yildiz, G. Mese, O. Yalcin-Ozuysal, H. C. Tekin, E. Ozcivici, *Sci. Rep.* **2018**, *8*, 7239. <https://doi.org/10.1038/s41598-018-25718-9>.
- [29] S. Tasoglu, C. H. Yu, V. Liudanskaya, S. Guven, C. Migliaresi, U. Demirci, *Adv. Healthcare Mater.* **2015**, *4*, 1469.
- [30] V. A. Parfenov, E. V. Koudan, E. A. Bulanova, P. A. Karalkin, F. D. Pereira, N. E. Norkin, A. D. Knyazeva, A. A. Gryadunova, O. F. Petrov, M. M. Vasiliev, M. I. Myasnikov, V. P. Chernikov, V. A. Kasyanov, A. Yu. Marchenkov, K. Brakke, Y. D. Khesuani, U. Demirci, V. A. Mironov, *Biofabrication* **2018**, *10*, 034104.
- [31] W. L. Haisler, D. M. Timm, J. A. Gage, H. Tseng, T. C. Killian, G. R. Souza, *Nat. Protoc.* **2013**, *8*, 1940.
- [32] N. S. Lewis, E. El Lewis, M. Mullin, H. Wheadon, M. J. Dalby, C. C. Berry, *J. Tissue Eng.* **2017**, *8*, 204173141770442.
- [33] A. Ito, K. Ino, M. Hayashida, T. Kobayashi, H. Matsunuma, H. Kagami, M. Ueda, H. Honda, *Tissue Eng.* **2005**, *11*, 1553.
- [34] M. Rogosnitzky, S. Branch, *BioMetals* **2016**, *29*, 365.
- [35] L. Ye, Z. Shi, H. Liu, X. Yang, K. Wang, *J. Rare Earths* **2011**, *29*, 178.
- [36] A. Krokmal, O. Sapozhnikov, E. Koudan, S. Tsysar, Y. Khesuani, V. Parfenov, in *Proc. Meet. Acoust.*, Acoustical Society Of America, **2019**, p. 020006.
- [37] V. A. Parfenov, V. A. Mironov, K. A. van Kampen, P. A. Karalkin, E. V. Koudan, F. D. Pereira, S. V. Petrov, E. K. Nezhurina, O. F. Petrov, M. Myasnikov, F. X. Walboomers, H. Engelkamp, P. Christiane, Y. D. Khesuani, L. Moroni, C. Mota, *Biofabrication* **2020**, <https://doi.org/10.1088/1758-5090/ab7554>.
- [38] A. Krüger-Genge, A. Blocki, R. P. Franke, F. Jung, *Int. J. Mol. Sci.* **2019**, *20*, 4411.
- [39] Y. Jung, H. Ji, Z. Chen, H. Fai Chan, L. Atchison, B. Klitzman, G. Truskey, K. W. Leong, *Sci. Rep.* **2015**, *5*, 15116. <https://doi.org/10.1038/srep15116>.
- [40] H. Tseng, J. A. Gage, W. L. Haisler, S. K. Neeley, T. Shen, C. Hebel, H. G. Barthlow, M. Wagoner, G. R. Souza, *Sci. Rep.* **2016**, *6*, 30640.
- [41] T. Okamoto-Koizumi, M. Takeda, T. Komeyama, A. Hatano, M. Tamaki, T. Mizusawa, T. Tsutsui, K. Obara, Y. Tomita, K. Arai, K. Takahashi, *Clin. Sci.* **1999**, *96*, 397.
- [42] M. J. Susienka, B. T. Wilks, J. R. Morgan, *Biofabrication* **2016**, *8*, 045003.
- [43] T. Roby, S. Olsen, J. Nagatomi, *Ann. Biomed. Eng.* **2008**, *36*, 1744.
- [44] A. Fusto, L. A. Moyle, P. M. Gilbert, E. Pegoraro, *Dis. Models Mech.* **2019**, *12*, dmm041368.
- [45] I. Holland, J. Logan, J. Shi, C. McCormick, D. Liu, W. Shu, *Bio-Des. Manuf.* **2018**, *1*, 89.
- [46] M. V. Berry, A. K. Geim, *Eur. J. Phys.* **1997**, *18*, 307.
- [47] J. Tavakkoli, D. Cathignol, R. Souchon, O. A. Sapozhnikov, *J. Acoust. Soc. Am.* **1998**, *104*, 2061.
- [48] O. A. Sapozhnikov, M. R. Bailey, *J. Acoust. Soc. Am.* **2013**, *133*, 661.
- [49] L. P. Gor'kov, *Sov. Phys. Dokl.* **1962**, *6*, 773.
- [50] C. R. Mol, *J. Acoust. Soc. Am.* **1982**, *71*, 455.